

## Probing boundary-corrections to Nambu-Goto open string energy levels in 3d $SU(2)$ gauge theory

---

**Bastian B. Brandt**

*Institut für Kernphysik, Johannes Gutenberg-Universität Mainz,  
Johann-Joachim-Becher-Weg 45, D-55128 Mainz*

*E-mail:* [brandt@kph.uni-mainz.de](mailto:brandt@kph.uni-mainz.de)

**ABSTRACT:** We measure the energy levels of the excitations of the flux tube between static quark and antiquark in three-dimensional  $SU(2)$  gauge theory. Combining exponential error reduction techniques and a variational method we are able to reduce the errors for the excited states significantly and to extract excited states in distinct parity and charge conjugation channels. It is conjectured that the infrared behavior (at large  $q\bar{q}$  separation  $R$ ) of the flux tube is governed by an effective string theory. Indeed previous simulations show good agreement between lattice data and predictions from Nambu-Goto string theory. Recently, new results on the effective string theory obtained corrections to the Nambu-Goto predictions and showed that for the open string in three dimensions first corrections should appear at order  $1/R^4$ . They correspond to boundary terms in the worldsheet field theory. These corrections are presumably small for the ground state, but significantly larger for the excited states and lift the degeneracies of the free theory. Assuming this functional form of the correction, we obtain for the coefficient  $b_2 = -0.5(2)(2)$ .

**KEYWORDS:** Lattice Gauge Field Theories, Confinement, Bosonic Strings, Long Strings

**ARXIV EPRINT:** [1010.3625](https://arxiv.org/abs/1010.3625)

---

## Contents

<b>1</b>	<b>Introduction</b>	<b>1</b>
<b>2</b>	<b>Corrections to Nambu-Goto from boundary terms</b>	<b>3</b>
<b>3</b>	<b>Details of the simulations</b>	<b>4</b>
3.1	Extraction of the energy spectrum	5
3.1.1	Extraction of eigenvalues	5
3.1.2	Groundstate energies in a given channel	6
3.1.3	Excited states in a given channel	7
3.1.4	Energy differences	7
3.2	Algorithm and simulation parameters	8
3.3	Sources of systematic effects	9
3.3.1	Finite volume effects	9
3.3.2	Control of the fits	9
<b>4</b>	<b>Results of the simulations</b>	<b>10</b>
<b>5</b>	<b>Discussion of <math>1/R^4</math> corrections</b>	<b>13</b>
<b>6</b>	<b>Conclusions</b>	<b>17</b>

---

## 1 Introduction

The formation of a flux tube between static quark and antiquark in the QCD vacuum, leads to a linearly rising potential and is one of the possible mechanisms to describe quark confinement. Simulations over the last years strongly support this picture (for a review see [1]). It is conjectured that at large distances  $R$  the dynamics of the flux tube is governed by an effective string theory, describing the properties of strong interactions in the infrared limit. The construction of models for these QCD strings in terms of open bosonic string theories have been attempted for a long time [2]. Today there are two different possible approaches for consistent effective string theories. The first idea, due to Polchinski and Strominger [3], was to construct an action consisting of all terms invariant under conformal transformations that avoids the conformal anomaly in an arbitrary number of dimensions. The first analysis of the closed string spectrum to  $\mathcal{O}(R^{-1})$  was extended up to and including  $\mathcal{O}(R^{-5})$  in [4–12], showing that the spectrum is equivalent to the spectrum of Nambu-Goto string theory (NG) [13, 14]

$$E_n^{NG}(R) = \sigma R \sqrt{1 + \frac{2\pi}{\sigma R^2} \left( n - \frac{1}{24} (d-2) \right)}, \quad (1.1)$$

at least to that order.

The other approach is due to Lüscher and Weisz [15, 16], using an action consisting of all possible terms constructed directly from the transverse degrees of freedom. The corresponding coupling constants are fixed through the duality between open and closed strings wrapping around a spatial dimension, which is valid in the presence of at least one compactified spatial dimension of length  $R$ . Recently their work was extended to even higher orders in  $1/R$  and to the open string case [17–19], using the  $SO(1 | d - 1)$  Lorentz symmetry to constrain additional coupling constants (see also [20]). Leading order corrections to the closed string spectrum in  $d > 2 + 1$  possibly appear at order  $\mathcal{O}(R^{-5})$  for the excited states and at  $\mathcal{O}(R^{-7})$  for the ground state. For the energy spectrum of the open string the picture is different due to boundary terms in the effective action. Indeed it turns out that first corrections to all states may already appear at  $\mathcal{O}(R^{-4})$ , also for  $d = 2 + 1$ . In addition, there are possible corrections at  $\mathcal{O}(R^{-5})$  for  $d > 2 + 1$ . It is thus natural to look for boundary corrections in the  $d = 2 + 1$  theory, since these are the only ones contributing up to  $\mathcal{O}(R^{-6})$  at least.

The predictions from these effective theories can be tested by comparison to simulations of pure Yang-Mills theories and a lot of studies were done using different theories in  $2 + 1$  and  $3 + 1$  dimensions, see [21] and references therein. In this context it is important to note, that liftings of degeneracy in the open string energy levels for  $d = 3 + 1$  in pure  $SU(3)$  gauge theory were already reported in [22–24]. For recent results on the closed string spectrum in  $2 + 1$  and  $3 + 1$  dimensional  $SU(N)$  gauge theory see [25, 26]. In the last years accurate measurements for the width of the flux tube became feasible as well and results with improved systematics and high accuracy coincide with the NG predictions for this quantity [27, 28].

It is an ambitious project to compare the energy spectrum of the flux tube with the predictions of the effective model. The stringy behavior is expected to set in at relatively large distances and the expected deviations from NG energy levels are small. Thus one has to measure a small effect at relatively large energies. In addition one has to control systematic effects as e.g. contributions from excited states and effects coming from finite extent of the lattice. Indeed most simulations so far haven't been able to reduce the errors and to control the systematic effects sufficiently at the same time. This is especially true for open strings with Dirichlet boundary conditions, corresponding to the excited states of a flux tube between static quark and antiquark. The corresponding energy spectrum can be explored using Wilson loops, but large temporal extent is needed to ensure a sufficient suppression of contaminations from excited states.

In [29, 30] a new method was proposed to measure large loops with high accuracy, based on the Lüscher-Weisz multilevel algorithm [31], and has been applied to the spectrum of the flux tube in three-dimensional  $SU(2)$  gauge theory. In this study this method is combined with a variational method to extract excited state energies in a specific  $(C, P)$ -channel and reduce excited state contaminations as much as possible. This enables us to extract the energy levels accurate enough to compare to the predictions from the effective theory. Again we use  $SU(2)$  gauge theory and work in three dimensions, but focus only on one lattice spacing at  $\beta = 5.0$  with a relatively large lattice spacing in terms of  $r_0$ , the Sommer

scale [32]. Simulating three instead of four dimensions is convenient because simulations are much faster and  $1/R^5$  corrections to the NG energy levels are absent in the three-dimensional theory.

The paper is organised as follows: In the next section we begin by summarising the corrections to the Nambu-Goto energy levels and lay the groundwork for the comparison to the measurements. In section 3 we turn to the details of the simulations, describe the extraction of the excited states and the control of systematic errors. In section 4 we discuss our results and compare to the NG predictions. In section 5 we compare to the boundary corrections and finally draw our conclusions in the last section.

## 2 Corrections to Nambu-Goto from boundary terms

In this section we discuss the boundary corrections to the energy spectrum of open strings in  $d = 2 + 1$ . To keep things simple, we only discuss the main points and adopt the notation from [18, 19]. As shown there, the only additional contribution to NG energy levels to  $\mathcal{O}(R^{-5})$  in the effective theory in  $2 + 1$  dimensions is the contribution of a boundary term, leading to the Hamiltonian

$$H'_2 = -b_2 \frac{\pi^3}{R^4} \left( 4 \sum_{n=1}^{\infty} n^2 \alpha_{-n} \alpha_n + \frac{d-2}{60} \right). \quad (2.1)$$

The states of the Fock space contributing to the three lowest energy levels, denoted by  $E_{n,i}$ , where  $n$  is the energy level in the free theory and  $i$  is the index for the degenerate states at that level, are given by:

energy	$ n, i\rangle$	representation	$(C, P)$
$E_0$	$ 0\rangle$	$\mathbf{1}  0\rangle$	$(+, +)$
$E_1$	$ 1\rangle$	$\alpha_{-1}  0\rangle$	$(+, -)$
$E_{2,1}$	$ 2, 1\rangle$	$\alpha_{-1} \alpha_{-1}  0\rangle$	$(+, +)$
$E_{2,2}$	$ 2, 2\rangle$	$\alpha_{-2}  0\rangle$	$(-, -)$

Here  $P$  is the parity quantum number of the state and  $C$  what we call the quantum number of charge conjugation (called transverse and longitudinal parity respectively in [26]). To be precise:  $C$  is the exchange between quark and antiquark, combined with a change in the direction of the gluonic flow. Using the commutation relations

$$[\alpha_n, \alpha_{-n}] = n \delta_{nm} \quad (2.2)$$

it is straightforward to compute the corrections to the NG energies  $\epsilon_{n,i}$  of these states due to the Hamiltonian (2.1). The corrections are given by:

$$\begin{aligned}
\epsilon_0 &= -b_2 \frac{\pi^3}{R^4} \frac{(d-2)}{60} \\
\epsilon_1 &= -b_2 \frac{\pi^3}{R^4} \left( 4 + \frac{(d-2)}{60} \right) \\
\epsilon_{2,1} &= -b_2 \frac{\pi^3}{R^4} \left( 8 + \frac{(d-2)}{60} \right) \\
\epsilon_{2,2} &= -b_2 \frac{\pi^3}{R^4} \left( 32 + \frac{(d-2)}{60} \right)
\end{aligned} \tag{2.3}$$

As we see, already the ground state obtains a  $\mathcal{O}(R^{-4})$  correction from the boundary terms, which is nevertheless strongly suppressed by a factor  $1/60$  and therefore hardly visible in our simulation, except for the unlikely case that  $b_2$  is large. Nevertheless it might be visible in high accuracy simulations for the ground state, as e.g. performed in [33, 34]. The corrections to the excited states are enhanced by a factor 240 or more compared to the ground state correction and are therefore much easier to detect, even though it is harder to extract these states numerically. In addition the degeneracy of the states at  $n = 2$  in the free theory is lifted and the magnitude of the corrections to the two formerly degenerate states differ by roughly a factor of 4.

Important for the comparison between measurements and the predictions is the radius of convergence of the expansion of the string energy levels in  $1/R$ , which can be estimated by  $x_c = 1/\lambda$ , the radius of convergence for the expansion of  $\sqrt{1+\lambda x}$  around  $x = 0$ . In the effective string theory the radius of convergence corresponds to a critical length  $R_c \sqrt{\sigma} = \sqrt{1/x_c}$  below which the expansion of the square root ceases to be convergent. For closed strings this critical length is relatively large,  $R_c \sqrt{\sigma} \gtrsim 3.4$  for  $d = 2 + 1$ , while for the open string we have

$$R_c \sqrt{\sigma}|_{n=1} = 2.45, \quad R_c \sqrt{\sigma}|_{n=2} = 3.51. \tag{2.4}$$

As can be seen from [30, 35, 36], extracting the energies of a flux tube of this length is possible, especially for the first excited state. Nevertheless the coefficient  $b_2$  is not known *ab initio* and we have to extract it from the data. We discuss the extraction of  $b_2$  and the results in section 5.

### 3 Details of the simulations

Wilson loops are the observables suited to consider the excited states of the flux tube and were already used in [22–24] and [29, 30, 35, 36] to extract the spectrum of the excitations. In this study, we combine the use of correlation matrices with the error reduction method from [29, 30] to extract the excitations spectrum in the  $(C, P)$ -channels from large Wilson loops and suppress contributions from other excited states as much as possible.

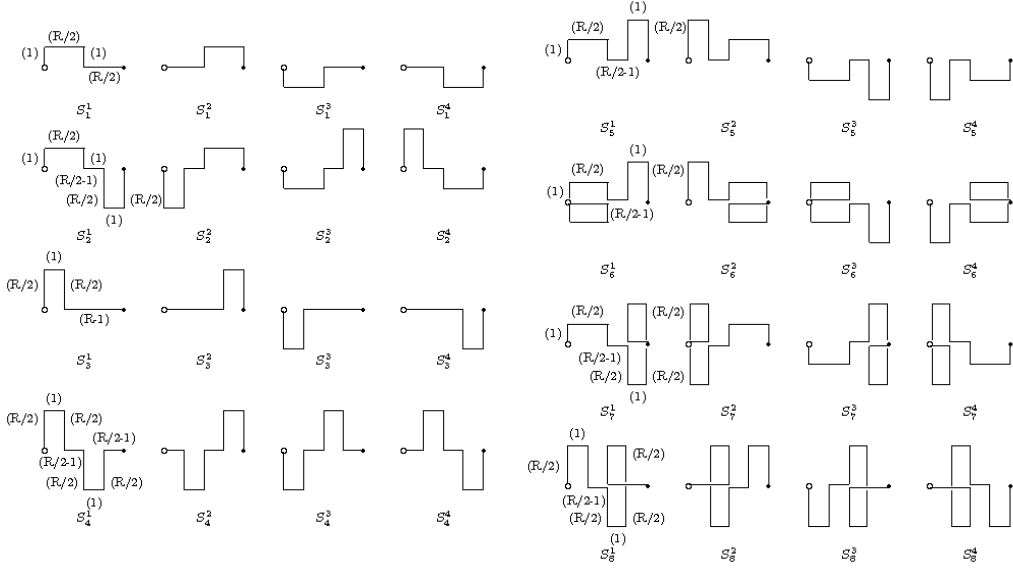


**Figure 1.** Sets of operators to construct the correlation matrices in different  $(C, P)$  channels.

### 3.1 Extraction of the energy spectrum

#### 3.1.1 Extraction of eigenvalues

To extract the energy spectrum we use 8 different operator sets, shown in figure 1. From these sets we first construct  $(C, P)$ -projectors, given by the linear combinations (see also [30])

$$\begin{aligned}
 S_i^{++} &= S_i^1 + S_i^2 + S_i^3 + S_i^4 \\
 S_i^{+-} &= S_i^1 + S_i^2 - S_i^3 - S_i^4 \\
 S_i^{--} &= S_i^1 - S_i^2 - S_i^3 + S_i^4 \\
 S_i^{-+} &= S_i^1 - S_i^2 + S_i^3 - S_i^4 .
 \end{aligned}
 \tag{3.1}$$

With these projectors we construct a correlation matrix in each of the  $(C, P)$ -channels.

To obtain the energies one has to extract the eigenvalues in the limit  $T \rightarrow \infty$ . Extracting these eigenvalues is a delicate topic, since loops with a temporal extent much larger than  $3r_0$  are out of reach with today's algorithms. In addition the number of operators  $N$  used to construct correlation matrices is finite, leading to the problem that even though one has extracted the eigenvalues carefully there might be a remaining mixing with states belonging to other energy levels. Usually one would use a generalised eigenvalue problem (GEVP), as discussed e.g. in [37]. The GEVP has the advantage that the excited states contributing to each of the eigenvalues start at  $n = N + 1$  as shown in [38]. In our case it is hardly possible to establish this method accurately, since the correlation matrix might be ill-conditioned even for the smallest values of  $T$ . This is especially an issue in the case of the correlation matrices in the  $(-, -)$  and  $(-, +)$ -channels, where the signal to noise ratio of the larger eigenvalues becomes very small. We therefore diagonalise the correlation matrices at each value of  $T$  separately to obtain the eigenvalues  $\lambda_n^{CP}(R, T)$  with  $n = 0, \dots, 7$ , using the  $QR$  reduction method (see e.g. [39]) and check explicitly the  $T$  dependence of

the overlaps between eigenvalues and operators. This method is analogous to the method used in [26], where a variational criterion has been applied at each value of  $T$  separately. For all states discussed in this study there is no significant change in the overlaps in the range of  $4 \leq T \leq 12$  and we do not expect to see any relicts of this in the data. In contrast to the case of the GEVP we now have a remaining mixing with each energy level in the channel, even though the mixing between the smallest eigenvalues should be suppressed if we have chosen the operators wisely. In [25] and [26] this mixing is minimised by using a very large number of basis states. Increasing the number of operators above a limit of around 50 is hardly possible in combination with our error reduction algorithm, since the needed computing resources grows drastically.

### 3.1.2 Groundstate energies in a given channel

In this study we mainly focus on the ground states of the  $(C, P)$ -channels, except for the first excited state in the  $(+, +)$ -channel, which is discussed in the next section. Each of the eigenvalues corresponding to the ground state in a channel now obeys the spectral representation

$$\lambda_0^{CP}(R, T) = \sum_{j=0}^{\infty} \beta_j^{CP}(R) e^{-E_j^{CP}(R) T} , \quad (3.2)$$

where  $E_j^{CP}$  are the energies in the  $(C, P)$ -channel and  $\beta_j^{CP}$  the overlaps with the eigenstate.

If the excited states are suppressed sufficiently, we can extract the corresponding energies using the asymptotic behavior

$$-\ln(\lambda_0^{CP}(R, T)) = \bar{E}_0^{CP}(R) T - \ln(\beta_0^{CP}(R)) , \quad (3.3)$$

which is exact in the limit  $T \rightarrow \infty$ . In practice  $\bar{E}_0^{CP}(R)$  is obtained by fitting the data to (3.3) together with the logarithm as an additional fit parameter. These energies are called naïve from now on, because contaminations from excited states are neglected.

Unfortunately the simulations have shown that the suppression of the excited states is not sufficient with the loop sizes in reach with the present methods of error reduction. This is especially crucial for larger values of  $R$  as shown in section 4. It is therefore mandatory to take the corrections into account. This can be done by fitting the eigenvalues for different temporal extents  $T_a$  and  $T_b$  to the leading order formula (see also [29, 30, 35, 36])

$$\begin{aligned} -\frac{1}{T_b - T_a} \ln \left[ \frac{\lambda_0^{CP}(R, T_b)}{\lambda_0^{CP}(R, T_a)} \right] &= E_0^{CP}(R) + \frac{1}{T_b - T_a} \alpha^{CP}(R) e^{-\delta^{CP}(R) T_a} \\ &\times \left( 1 - e^{-\delta^{CP}(R) (T_b - T_a)} \right) . \end{aligned} \quad (3.4)$$

Here  $T_a < T_b$ ,  $\alpha^{CP}(R) = \beta_1^{CP}(R)/\beta_0^{CP}(R)$  and  $\delta^{CP}(R)$  is the energy gap to the first excited state in the channel. The energies  $E_0^{CP}(R)$  are called corrected from now on and are obtained as fit parameters together with the  $\alpha$ 's and  $\delta$ 's from fits to all possible combinations of  $T_a$  and  $T_b$ . The control of these fits is discussed in more detail in section 3.3.2.

### 3.1.3 Excited states in a given channel

For an eigenvalue corresponding to an excited state in a channel the situation is different due to possible mixings with states of smaller energy. The only excited state in a channel used in this study is the first excited state in the  $(+, +)$ -channel on which we focus in this section. The only state with smaller energy contributing is the corresponding ground state, whose energy  $E_0^{++}(R)$  can be extracted with the procedure described above. For the naïve energy  $\bar{E}_1^{++}$  we can use a fit to the form (3.3), since mixings with other energy levels are neglected in this quantity. Nevertheless the extraction of the corrected energy  $E_1^{++}$  needs some additional discussion.

A fit to the form (3.4) removes the contaminations from states with larger energy values. This remains true for excited states in a channel, but one has to include also the corrections coming from states with smaller energy. For the state  $E_1^{++}$  we can check the contribution of the state  $E_0^{++}$  by adding the corresponding term

$$\frac{\gamma(R)}{T_b - T_a} e^{(E_1^{++}(R) - E_0^{++}(R)) T_a} \left( 1 - e^{(E_1^{++}(R) - E_0^{++}(R)) (T_b - T_a)} \right) \quad (3.5)$$

to the fit (3.4). Performing a fit using (3.4) together with (3.5) shows, that the contribution of  $E_0^{++}(R)$  should be well below our statistical errors, since  $\gamma$  is in all cases a number below  $10^{-4}$ , so that the total contribution of (3.5) is below  $5 \cdot 10^{-3}$ , well below the statistical errors for the corrected energy  $E_1^{++}$ . The other fit parameters agree well with the parameters obtained by a fit to the form (3.4) within the statistical errors. As corrected values for  $E_1^{++}(R)$  we thus use the results from a fit to the form (3.4) and neglect the contribution of the ground state.

### 3.1.4 Energy differences

The extraction of the energy differences can be treated independently from the extraction of the total energies. In this way the energy differences might serve as an independent check of the asymptotic results for the total energies. Using (3.2) one can obtain for the naïve energy differences the formula

$$-\ln \left( \frac{\lambda_n^{CP}(R, T)}{\lambda_m^{CP'}(R, T)} \right) = \left[ \bar{E}_n^{CP}(R) - \bar{E}_m^{CP'}(R) \right] T - \ln \left( \frac{\beta_{n,0}^{CP}}{\beta_{m,0}^{CP'}} \right), \quad (3.6)$$

which is similar to (3.3) for the total energies. This formula for naïve differences is also valid for the differences between excited states in a given  $(C, P)$ -channel.

As before we are mainly interested in the differences between the energies of the ground states in different channels. For these the leading order formula for the corresponding corrected energy difference is the same as in [30],

$$\begin{aligned} & - \frac{1}{T_b - T_a} \ln \left[ \frac{\lambda_0^{CP}(R, T_b) \lambda_0^{CP'}(R, T_a)}{\lambda_0^{CP}(R, T_a) \lambda_0^{CP'}(R, T_b)} \right] \\ & = \left[ E_0^{CP}(R) - E_0^{CP'}(R) \right] + \frac{1}{T_b - T_a} \bar{\alpha}(R) e^{-\bar{\delta}(R) T_a} \left( 1 - e^{-\bar{\delta}(R) (T_b - T_a)} \right), \end{aligned} \quad (3.7)$$



$\beta$	$r_0/a$	$R$	$T$	$T/r_0$	$t_s$	lat size	$N_s$	$N_t$	# meas
5.0	3.9536(3)	4-12	4	1.01	2	$32^3$	16000	1500	3200
			6	1.52		$36^3$		2000	3200
			8	2.02		$40^3$		6000	5100
			10	2.53		$40^3$		12000	6400
			12	3.04		$48^3$		16000	8600

**Table 1.** Run parameters of the simulations.  $r_0$  is the Sommer parameter,  $t_s$  the temporal extent of the sublattices in the LW algorithm,  $N_s$  the number of updates of the sublattice containing the spatial operators and  $N_t$  the number of updates of the sublattices containing only the time transporters.

where  $\bar{\alpha}$  is a suitable combination of the overlaps and  $\bar{\delta}$  corresponds to the energy gap to the next excited state in the channel  $CP'$  (which is equivalent to the gap in the channel  $CP$  to leading order in  $1/R$ ). In addition to the energy differences between the ground state energies we are also interested in the energy differences between  $E_1^{++}$  and  $E_0^{++}$ . In this case the two terms corresponding to the mixing between  $E_1^{++}$  and  $E_0^{++}$  are a term of the form (3.5) and a term of the form

$$\begin{aligned} & \frac{\bar{\alpha}(R)}{T_b - T_a} \left( \frac{\gamma(R)}{\beta_0(R)} \right) e^{(E_1^{++}(R) - E_0^{++}(R) - \bar{\delta}(R)) T_a} \\ & \times \left( 1 - e^{(E_1^{++}(R) - E_0^{++}(R) - \bar{\delta}(R)) (T_b - T_a)} \right) \ll 10^{-4} \end{aligned} \quad (3.8)$$

The total contribution of these terms is below  $5 \cdot 10^{-3}$  and thus negligible compared to the statistical errors. We therefore use a fit to the form (3.7) for that difference, too.

### 3.2 Algorithm and simulation parameters

The need for suppression of the contributions from excited states and the onset of string-like behavior in the large  $R$  regime demands large Wilson loops, and an efficient algorithm with sufficient error reduction for large loops is needed to extract the spectrum with high accuracy. The algorithm used in this study is a variation of the Lüscher Weisz algorithm [31] and discussed in detail in [30].

Our simulations were done using the  $SU(2)$  Wilson plaquette action in 2+1 dimensions at  $\beta = 5.0$ . The Sommer parameter is known e.g. from [29, 35, 36] and listed together with the simulation parameters in table 1. In fact the lattice spacing in terms of the Sommer parameter is not very small, but a comparison from the results of the four different  $\beta$  values from [29] and [30] shows that there is not much movement in the energies expressed in terms of  $r_0$  over the whole range of  $5.0 \leq \beta \leq 12.5$ . We therefore expect that our results are relevant for the continuum as well. In contrast to [29, 30, 35, 36], we work with 5 different temporal extents instead of 4, which leads to strong improvements in the extraction of the asymptotic behavior and the control of contaminations from excited states via (3.4) and (3.7).

Statistical errors are estimated using the usual binned jackknife method with 50 bins for all measurements. We explicitly checked that none of the error estimates varies more than a few percent with bin size.

### 3.3 Sources of systematic effects

#### 3.3.1 Finite volume effects

The first class of sources of systematic errors in addition to the ones discussed in section 3.1 is due to finite extent  $L$  of the lattice. Here periodic boundary conditions are applied to the lattice, making it possible for the loops to interact with themselves by around-the-world glueball exchanges. In the string picture these exchanges corresponds to handles on the world sheet, wrapping around a compactified dimension. The contribution of such a handle to the signal of the Wilson loop takes the form

$$a(L') \exp(-m_G L') , \quad (3.9)$$

where  $L'$  is the length of the handle,  $m_G$  the mass of the lightest glueball (measured in [40] for  $SU(2)$  in  $d = 2 + 1$  and at  $\beta = 5.0$ ) and  $a(L')$  is the overlap with the loop. In principle these handles can wrap around any of the directions, but it is immediately clear from (3.9) that the main contribution comes from the direction that enables the shortest handle. Clearly this is the direction parallel to the spatial direction of the Wilson loop where  $L' = L - R$ . The main problem thus arises for Wilson loops with large values of  $R$ . For the case of our study,  $2 + 1$  dimensional  $SU(2)$  with  $\beta = 5.0$ , a test for finite volume effects with volumes of  $24^3$  and  $48^3$ , excited states up to  $n = 3$  and  $R \leq 12$  already exists [30]. Since no finite volume effects were visible in this test, we can conclude that  $a(L')$  is at most a factor of  $\mathcal{O}(1)$  and that we do not expect to suffer from any finite volume effects up to energy levels of  $n = 3$  at least.

#### 3.3.2 Control of the fits

In the analysis a lot of fitting is done in order to extract the energies and energy differences in the limit  $T \rightarrow \infty$  and to take the contaminations from excited states into account. For the control of systematic effects it is thus crucial to control these fits in several ways, since these are the biggest source for systematic errors in the final data.

Even though the fits (3.3) and (3.6) include only a linear fit function it might be that already these fits give biased results, since the more important points for the asymptotic behavior, the points from loops with large  $T$ , come with bigger statistical errors. This might lead to the problem that the fit is completely determined by the values at small  $T$ . As a check we plotted the data along with the resulting lines and checked the deviations from the line of the points at large  $T$ . Where the deviations were not at the percent level and below the statistical errors, we discarded the fit.

The second type of fits, eq. (3.4) and (3.7), are much harder to control, since these fits include nonlinear functions of two arguments. In addition the  $\chi^2/d.o.f.$  of these fits is usually very small and does not provide much information on the goodness of the fits. We thus apply two checks that were already discussed in [30]. We expect  $\alpha$  to be smaller than

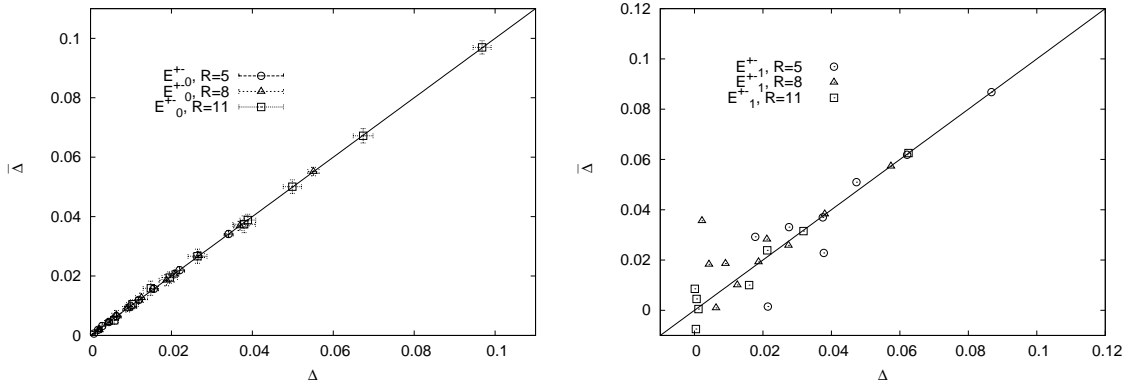


**Figure 2.** Cross check of the fits for the corrected energies (3.4) and energy differences (3.7): **Left:** Fits for  $E_0^{+-}$ ,  $R = 5, 8$  and  $11$ . These fits are expected to give reliable results. **Right:** Fits for  $E_1^{+-}$ ,  $R = 5, 8$  and  $11$ . These fits are regarded to be unreliable, since the points are clearly not following the  $\Delta = \bar{\Delta}$ -line. We have not plotted the error bars in the right fit, because they are large and confuse the picture.

the ratio of the degeneracies between the next excited state and the state considered and  $\delta$  to be of the order of the energy gap between the two. Wherever this criterion was not fulfilled we did not use the fits. The second check is a comparison between the expected corrections

$$\Delta = \frac{1}{T_b - T_a} \alpha_n^{CP}(R) e^{-\delta_n^{CP}(R) T_a} \left( 1 - e^{-\delta_n^{CP}(R) (T_b - T_a)} \right), \quad (3.10)$$

obtained with averaged parameters  $\alpha_n^{CP}$  and  $\delta_n^{CP}$ , and the difference

$$\bar{\Delta} = E_n^{CP}(R) + \frac{1}{T_b - T_a} \ln \left[ \frac{\lambda_n^{CP}(R, T_b)}{\lambda_n^{CP}(R, T_a)} \right], \quad (3.11)$$

for each  $R$  and all combinations of  $T_a$  and  $T_b$ . We expect to obtain  $\Delta = \bar{\Delta}$  for each  $R$ . The plot of  $\bar{\Delta}$  against  $\Delta$  for three examples where we expect the fits to work are shown on the left of figure 2, while on the right we show three examples where the fits are regarded to be unreliable. Similar checks were performed for the energy differences, too [30].

## 4 Results of the simulations

We list all results, naïve and corrected in tables 2 and 3, to enable other groups to use the data for comparisons. In this section we compare our data to the full NG energy spectrum (1.1) and its truncations in  $1/R^2$  to leading order (LO), next-to leading order (NLO) and next-to-next-to leading order (NNLO). The comparison to corrections from boundary terms is postponed to the next section.

In order to compare to the data we have to extract the string tension  $\sigma$  and fix an unphysical constant  $V_0$ . Since we expect corrections to appear with respect to the full NG prediction (as concluded e.g. in [26] and [19]), we fit the ground state data to the form

$$V(R) = \sigma R \sqrt{1 - \frac{\pi}{12 \sigma R^2}} + V_0. \quad (4.1)$$

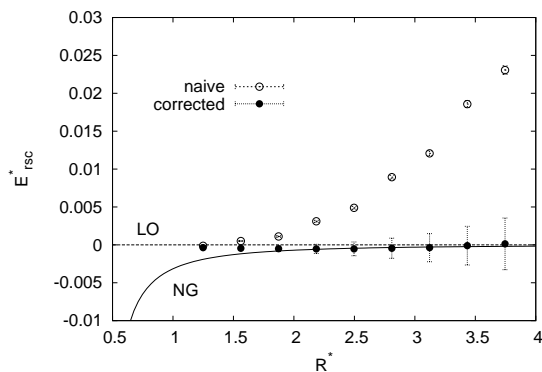


**Figure 3.** Results for the ground state rescaled such that  $E_0^{*,LO} \equiv 0$ . The lines are the LO and NG predictions as defined by (1.1) in dimensionless quantities, eq. (4.3).

$R$	$E_0^{++} = E_0$		$E_0^{+-} = E_1$		$E_1^{++} = E_{2,1}$		$E_0^{--} = E_{2,2}$	
	naïve	corr	naïve	corr	naïve	corr	naïve	corr
4	0.57281(3)	0.5716(1)	1.1278(2)	1.118(1)	1.452(2)	1.35(6)	1.5056(9)	—
5	0.67623(4)	0.6756(2)	1.1643(2)	1.152(1)	1.491(1)	1.41(2)	1.5110(8)	1.477(12)
6	0.77831(5)	0.7775(2)	1.2115(2)	1.198(1)	1.516(1)	1.45(2)	1.5296(8)	1.511(7)
7	0.87969(7)	0.8781(3)	1.2735(2)	1.255(1)	1.581(1)	1.51(1)	1.5674(7)	1.549(6)
8	0.98000(8)	0.9779(4)	1.3387(2)	1.318(2)	1.648(1)	1.56(1)	1.6137(7)	1.595(5)
9	1.08047(9)	1.0772(5)	1.4159(2)	1.387(2)	1.731(2)	1.62(1)	1.6685(7)	1.648(5)
10	1.18005(11)	1.1761(6)	1.4899(2)	1.460(2)	1.846(2)	1.69(2)	1.7296(8)	1.709(4)
11	1.28020(13)	1.2749(8)	1.5766(2)	1.537(2)	1.940(3)	1.76(2)	1.7946(9)	1.774(4)
12	1.37937(15)	1.3734(9)	1.6559(3)	1.616(3)	2.046(4)	1.84(4)	1.8644(9)	1.843(3)

**Table 2.** Results for the total energies in lattice units. In addition to the corrected data, which are our final results, we also list the naïve results. They give upper bounds for future simulations and illustrate the effect of contaminations from excited states. Note that also the naïve energies are already asymptotic results for  $T \rightarrow \infty$ , neglecting the contaminations.

Since we expect string like behavior to set in at  $\sim 2 r_0$  [30, 33, 34], we omit the first three points in the fit and obtain

$$\sigma = 0.0975(2) \quad \text{and} \quad V_0 = 0.2148(7) . \quad (4.2)$$

This result for  $\sigma$  is consistent with the value from [33, 34] within the error bars. The error bars are much larger in our case, which is no surprise since our aim is not to obtain the ground state energy and the string tension with high accuracy and our setup is not tuned to reduce this error in particular. From now on we are going to use the dimensionless quantities

$$R^* \equiv \sqrt{\sigma} R \quad \text{and} \quad E^* \equiv (E - V_0) / \sqrt{\sigma} \quad (4.3)$$

for plotting and comparisons to the predictions.

We plot the naïve and corrected results for the ground state in figure 3. In the plots we have rescaled the energies such that  $E_n^{*,LO} \equiv n$ , i.e.

$$E_{n,rsc}^*(R^*) = (E_n^*(R^*) - R^*) \frac{R^*}{\pi} + \frac{1}{24} , \quad (4.4)$$

$R$	$E_0^{+-} - E_0^{++}$ $= \Delta E_{10}$		$E_1^{++} - E_0^{++}$ $= \Delta E_{20}$		$E_0^{--} - E_0^{++}$ $= \Delta E_{20}$		$E_1^{++} - E_0^{+-}$ $= \Delta E_{21}$	
	naïve	corr	naïve	corr	naïve	corr	naïve	corr
4	0.5558(2)	0.547(1)	—	—	0.9334(9)	—	—	—
5	0.4879(2)	0.476(2)	0.814(1)	0.734(18)	0.8341(8)	0.800(12)	0.319(1)	—
6	0.4330(2)	0.421(2)	0.736(1)	0.672(14)	0.7506(8)	0.733(7)	0.296(1)	0.25(2)
7	0.3936(2)	0.377(2)	0.699(2)	0.628(11)	0.6867(7)	0.671(6)	0.296(2)	0.25(1)
8	0.3584(2)	0.340(2)	0.666(1)	0.585(9)	0.6325(7)	0.617(5)	0.299(1)	0.24(1)
9	0.3351(2)	0.310(2)	0.648(2)	0.539(11)	0.5684(8)	0.571(5)	0.302(2)	0.23(1)
10	0.3094(2)	0.283(2)	—	0.513(16)	0.5477(8)	0.533(4)	—	0.23(2)
11	0.2956(2)	0.261(3)	—	0.483(19)	0.5122(9)	0.499(3)	—	0.22(2)
12	0.2757(2)	0.242(3)	—	0.467(35)	0.4828(9)	0.469(3)	—	0.22(4)

**Table 3.** Results for the energy differences in lattice units. As in table 2 we list corrected and naïve results. For some differences we were able to obtain corrected but no naïve results. This is due to the fact that the contaminations from excited states are large and the data points for the fit (3.6) do not lie on a straight line, whereas the fit (3.7) still works well.

to provide visibility of small effects. We see a clear splitting between the naïve and the corrected results, which increases when we go to larger values of  $R^*$ . The effect becomes even more severe when we go to the excited states, as shown for energy level  $E_1$  in figure 4 (top left). We can also see the approximate linear asymptotic behavior of the rescaled naïve energies when going to large  $R$  values, which was seen in [22–24], too. The asymptotic behavior of the corrected energies is different and we conclude that the behavior of the naïve energies is due to contributions from excited states and does not reflect the physical asymptotic behavior of the energies for large  $R$ . When we look at the predictions for the energy gaps from (1.1) and its truncations it is easy to see why the excited state contamination is enhanced. The energy gaps to the excited states decrease roughly like  $1/R$ , thus the damping with  $T$  is reduced in eq. (3.2) when going to larger  $R$  and more excited states contribute to the contamination. In the following we therefore only use corrected results for the discussions.

The results for  $E_1^{++}$  and  $E_0^{--}$ , belonging to the second excited state, are shown in figure 4 (top right). It is remarkable that with the new method and 5 different temporal extents we were able to reduce the errors for the corrected values of the ground state in the  $(+, -)$ -channel by a factor of more than two and to obtain corrected results for the groundstate in the  $(-, -)$ -channel with an accuracy better than that of the results for the ground state of the  $(+, -)$ -channel in [30]. The error bars of the first excited state in the  $(+, +)$ -channel are almost an order of magnitude bigger than the error bars from the ground state of the  $(-, -)$ -channel, but nevertheless we see a 2 – 4 sigma splitting up to  $R^* \approx 3$ . At that point the error of  $E_1^{++}$  becomes to large to distinguish between the two.

The energy differences are listed in table 3. They have the advantage that the comparison to the predictions does not involve the unknown constant  $V_0$  from eq. (4.1) and that they are more sensitive to subleading properties of the flux tube. In figure 4 we show the difference  $E_0^{+-} - E_0^{++}$  (left bottom), corresponding to the free difference  $\Delta E_{10}$ , and the

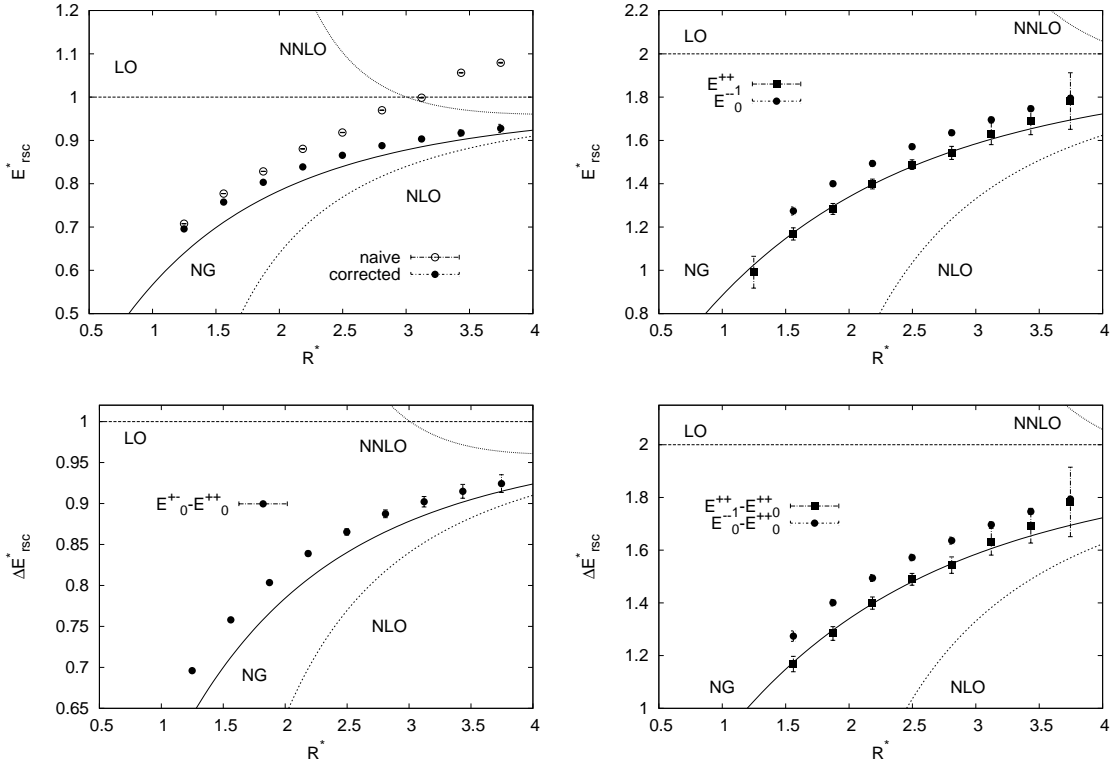


**Figure 4.** **Top:** Results for the first (left) and second excited state (right), rescaled such that  $E_n^{*,LO} \equiv n$ . **Bottom:** Results for the energy differences corresponding to  $\Delta E_{10}$  (left) and  $\Delta E_{20}$  (right) in the free theory. The data is rescaled such that  $\Delta E_{nm}^{*,LO} = n - m$ .

differences  $E_1^{++} - E_0^{++}$  and  $E_0^{--} - E_0^{++}$  (right bottom), corresponding to the free difference  $\Delta E_{20}$ . We see a similar error reduction as for the absolute energy values compared to [30].

The qualitative agreement between the data and the NG predictions is remarkable down to very small values of  $R^*$ , where we do not expect the flux tube to have a string like shape and where the expansion of the string action in  $1/R^*$  is no longer expected to converge. These findings are in full agreement with other simulations, e.g. [29, 30, 35, 36]. In addition they are consistent with the results from [15, 22–24] for smaller values of  $R^*$  and with the results obtained for closed strings [25, 26]. Even though the data follows the NG predictions qualitatively, we see a significant deviation for the absolute energies  $E_0^{+-}$  and  $E_0^{--}$ , as well as for the corresponding differences to the ground state, even for our largest values of  $R^*$ . We are going to compare these deviations to the boundary corrections in the next section. The  $E_1^{++}$  state is fully consistent with the NG prediction inside the error bars for all values of  $R^*$ , which is also true for the corresponding difference  $E_1^{++} - E_0^{++}$ .

## 5 Discussion of $1/R^4$ corrections

To compare the boundary corrections to the NG predictions with the data, we have to extract the unknown coefficient  $b_2$ . There is a hint from theory that  $b_2$  is negative and nonvanishing, coming from a computation of  $b_2$  for the case of a string ending on two d-

fit	$\sigma'$	$V'_0$	$b_2$	$\gamma_0$	$\gamma_1$	$\eta_0$	$\eta_1$	$\chi^2/d.o.f.$
1	0.0974(1)	0.2151(4)	-0.30(4)	—	—	—	—	0.79
2	0.0975(2)	0.2145(7)	-0.61(19)	2(3)	-2(1)·10 <sup>3</sup>	—	—	0.04
3	0.0975(2)	0.2145(6)	-0.52(14)	—	—	14(11)	-11(6)·10 <sup>3</sup>	0.05
4	0.0975(2)	0.2146(7)	—	9(3)	12(3)·10 <sup>3</sup>	—	-7(2)·10 <sup>4</sup>	0.22

**Table 4.** Results for the combined fit of ground state and first excited state data to the form (5.1). The different fits are described in the text.

branes in confining gauge theories with a weakly curved holographic dual [18]. Corrections appears at all energy levels and we demand that  $b_2$  is consistent with all data above the critical distance as defined in section 2. We therefore use the ground state as well as the first excited state to extract  $b_2$  from a simultaneous fit. We also have to account for the possibility that the values for  $\sigma$  and  $V_0$  are changed due to the ground state correction. We thus use them again as free parameters denoted as  $\sigma'$  and  $V'_0$  to distinguish them from the values obtained in the last section.

It is known that, when fitting to a polynomial, the coefficient of the highest power of the polynomial in the fit receives a summed contribution from possible higher order terms. This spoils the reliability of the highest coefficient of the fit polynomial.  $b_2$  suffers from the same problem, since the fit function is a nonlinear function in  $\sigma'$  combined with a polynomial correction. To improve the reliability of the obtained value for  $b_2$  we include a correction term of higher order to each energy level. There are in general two possibilities at which order the next correction term might appear. At  $\mathcal{O}(R^{-6})$  if there are additional boundary terms in the effective action or at  $\mathcal{O}(R^{-7})$  if the next correction term is a regular (non-boundary) correction. To account for these possibilities we parametrise our fit functions for a simultaneous fit to the ground state and the first excited state as:

$$\begin{aligned}
E_0(R) &= \sigma' R \sqrt{1 - \frac{\pi}{12 \sigma' R^2}} - b_2 \frac{\pi^3}{60} \frac{1}{R^4} + \gamma_0 \frac{1}{R^6} + \eta_0 \frac{1}{R^7} + V'_0 \\
E_1(R) &= \sigma' R \sqrt{1 + \frac{23 \pi}{12 \sigma' R^2}} - b_2 \frac{241 \pi^3}{60} \frac{1}{R^4} + \gamma_1 \frac{1}{R^6} + \eta_1 \frac{1}{R^7} + V'_0,
\end{aligned} \tag{5.1}$$

To check the effect of the higher order terms we perform the following fits:

1. Set  $\gamma_i \equiv 0$  and  $\eta_i \equiv 0$ , use  $b_2$  as a fit parameter.
2. Set  $\eta_i \equiv 0$ , use  $b_2$  and  $\gamma_i$  as fit parameters.
3. Set  $\gamma_i \equiv 0$ , use  $b_2$  and  $\eta_i$  as fit parameters.
4. Set  $b_2 \equiv 0$  and  $\eta_0 \equiv 0$ , use  $\gamma_i$  and  $\eta_1$  as fit parameters.

In all cases  $\sigma'$  and  $V'_0$  are free parameters as well. The last fit accounts for the possibility that the coefficient  $b_2$  vanishes identically, which is not yet ruled out completely by theory and thus remains a possibility. In the fits we include all points except the one with smallest  $R$  for the ground state, and all points with  $R \geq 7$  for the first excited state, since we expect the data to be consistent with the effective string theory even for smaller values of  $R$  when

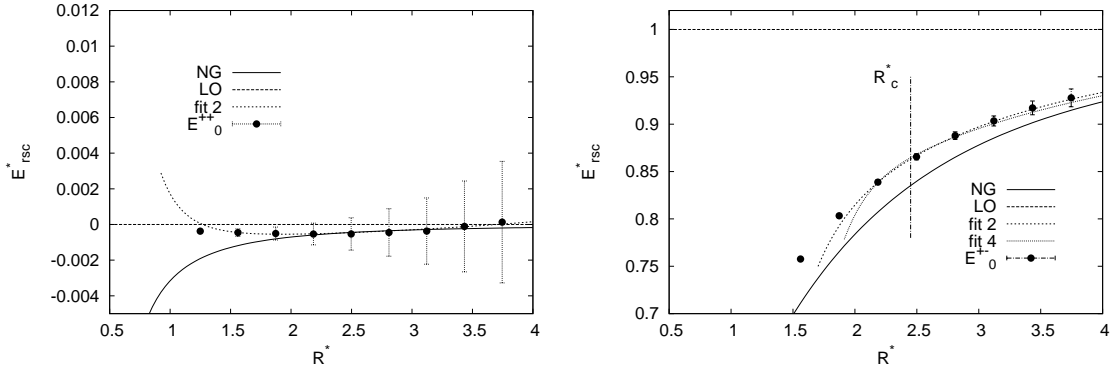


**Figure 5.** Comparison between fit 2 from table 4 and the data for the groundstate (left) and the first excited state (right). The data is rescaled as in the previous figures. The line marked with  $R_c^*$  is the line below which the expansion of the corresponding energy level in  $1/R^*$  ceases to be convergent.

the corrections are included. We exclude the data for the second excited state for the following reasons: Only the largest values of  $R^*$  are above the critical length below which the expansion of the energy ceases to be convergent for the second excited state (see eq. (2.4)) and one has to include four more fit parameters  $\gamma_{2,i}$  and  $\eta_{2,i}$  to the fits. Therefore the inclusion of the second excited state does not improve the information and the accuracy for  $b_2$ . We do not account for the possibility of correction terms below  $\mathcal{O}(R^{-4})$ , since we compare to the effective theory where these terms are explicitly ruled out.

We list the results of the fits in table 4. In all cases we see good agreement between  $\sigma'$  and  $V_0'$  and  $\sigma$  and  $V_0$  obtained in the previous section. This shows that the extraction of  $\sigma$  from the ground state is not sensitive to  $1/R^4$  corrections within the accuracy for the ground state data of our simulations. The result for  $b_2$  varies between fits 1 – 3, but is small and negative in all cases. We expect the results for  $b_2$  from the fits 2 and 3, including also the higher order terms, to be unbiased. In that case  $\gamma_0$  or  $\eta_0$  is practically consistent with zero, which is not surprising, since we expect the data for the ground state not to be accurate enough to make higher order corrections to a  $1/R^4$  correction visible.  $\gamma_1$  and  $\eta_1$  are nonzero but still small compared to the NG coefficient at  $\mathcal{O}(R^{-7})$ . Fit 4 seems to work as well but a relatively large nonvanishing boundary term at  $\mathcal{O}(R^{-6})$  is needed for the fit to work accurately. Nevertheless the corresponding  $\chi^2/d.o.f.$  is a magnitude bigger than for the fits 2 and 3 (even though it is still below one). Assuming that  $b_2$  does not vanish identically we find the data to be consistent with

$$b_2 = -0.5(2)(2) , \quad (5.2)$$

where the first error is statistical and the second reflects the systematical uncertainty, estimated from the variation of  $b_2$  between fits 1-3.

To compare to the data, we use fit 2 from table 4 and show the corresponding plots for the ground state and the first excited state in figure 5. We use  $\sigma$  and  $V_0$  as before (instead of  $\sigma'$  and  $V_0'$ ) to rescale the data points and show also the NG lines from the previous



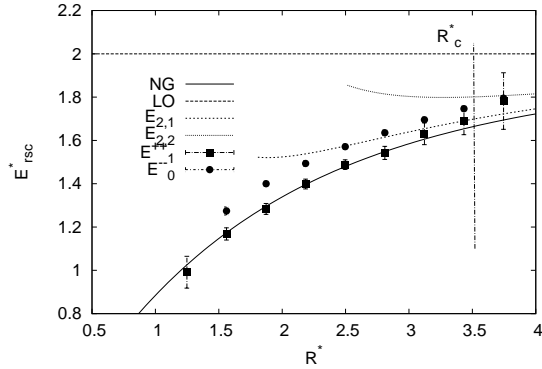


**Figure 6.** Comparison between the data for the second excited state and the corrected energy levels  $E_{2,1} = E_2^{NG} + \epsilon_{2,1}$  and  $E_{2,2} = E_2^{NG} + \epsilon_{2,2}$  with  $b_2$  obtained from fit 2. The data is rescaled as in the previous figures.

section for comparison. It is remarkable that we can accurately describe the corrections to two different energy states with a predicted splitting and a single coefficient. In addition we also show the resulting curve from fit 4 for the first excited state. We see that it deviates a little bit more from the data than the curve obtained from fit 2, but is well inside the error bars and describes the data as well.

Having fixed  $b_2$  through the fit (in this case fit 2), we now get a prediction for the two curves corresponding to the second excited state, where the degeneracy is lifted. We show the corresponding curves together with the data in figure 6. Additional terms of  $\mathcal{O}(R^{-6})$  or higher are excluded here, since we do not know anything about their coefficients and we expect the effects to be of minor importance at the present level of accuracy of the data. We see that the curve  $E_{2,1}$  stays below the  $E_{2,2}$  curve which is consistent with the behavior of the data. Nevertheless the data is closer to the NG curve when  $R^* < 3$ , which is well below  $R_c^*$  for the second excited state. Above  $R_c^*$  the data for  $E_0^{--}$  approaches the  $E_{2,2}$  curve, but it is not clear whether the behavior with increasing  $R^*$  remains consistent with the resulting curve. The data for  $E_1^{++}$  is consistent with the  $E_{2,1}$  curve already below  $R_c^*$ , but the error bars above  $R_c^*$  are too large to exclude the approach to any of the three curves.

The energy differences provide another check for the fits of this section. We show the curves obtained with the parameters from the fit above and the corresponding data in fig. 7. Above  $R_c^*$  we see perfect agreement between the  $\Delta E_{10}$  curve including the correction and the data. For  $\Delta E_{20}$  the picture is similar as for the total energies at  $n = 2$ , the data is roughly consistent with the predictions.

We can employ yet another independent check and use the splitting between first excited state and ground state directly to obtain  $b_2$ . In that case we can keep  $\sigma$  and  $V_0$  fixed, which are almost completely determined by the groundstate. When we include an additional correction term at  $\mathcal{O}(R^{-6})$  we obtain  $b_2 = -0.56(23)$  with  $\chi^2/d.o.f. = 0.03$ . This result is consistent with the results from the fits to the total energies. All in all, together with the hint from the effective theory that  $b_2$  should be nonvanishing, we consider the possibility of a vanishing  $1/R^4$  correction to be unlikely with our present data. The data

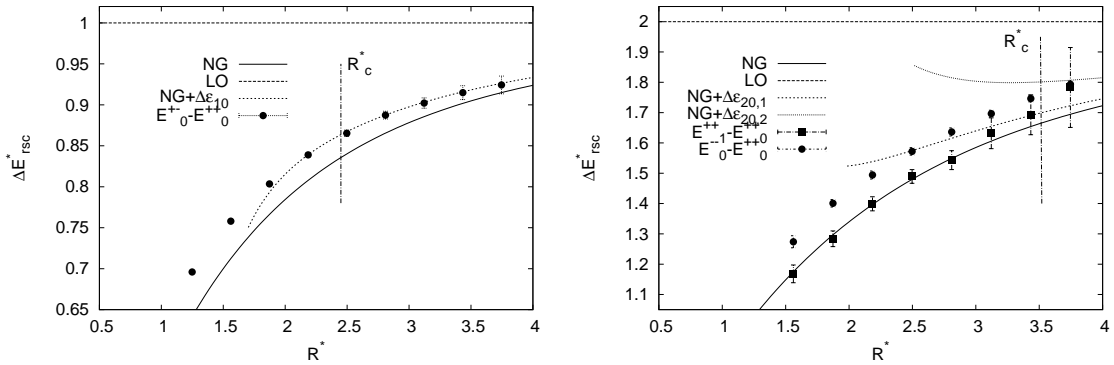


**Figure 7.** Comparison between the data for the energy differences  $\Delta E_{10}$  (left) and  $\Delta E_{20}$  (right) and the predictions with  $b_2$  obtained from fit 2. The data is rescaled as in the previous figures. We have used the abbreviations  $\Delta\epsilon_{10} = \epsilon_1 - \epsilon_0$ ,  $\Delta\epsilon_{20,1} = \epsilon_{2,1} - \epsilon_0$  and  $\Delta\epsilon_{20,2} = \epsilon_{2,2} - \epsilon_0$ .

for ground state and first excited state is well described by the predicted splitting of the effective theory with a single coefficient  $b_2$ . Also the behavior of the second excited state, which was not included in the fits, suits to the predictions.

## 6 Conclusions

In this article we have looked at the energies of the excited states of the flux tube between static quark and antiquark in three-dimensional  $SU(2)$  gauge theory, using a combination of the algorithm from [30] and a variational method. We studied  $q\bar{q}$  separations between 1 and  $3r_0$  and energy levels up to  $n = 2$ . We have discussed the main systematic effects entering the extraction of the excited states in detail, explained under which conditions we consider the results to be unaffected by any of these effects and included only those results in the analysis where systematics are under control. The only remaining systematic effect which is not investigated is the lattice spacing dependence, but results from [29, 30, 35, 36] suggests that the dependence on the lattice spacing is very mild. Using the correlation matrices in the  $(C, P)$  channels and 5 different temporal extents, we were able to further reduce the errors compared to [30] and to obtain a clear signal for the second excited state. In addition we were able to obtain results for the first excited state in the  $(+, +)$  channel, which is degenerate to the ground state in the  $(+, -)$  channel in the free theory. The effective string theory predicts a splitting of these formerly degenerate states and indeed we observe such a splitting in our data. In all cases we see the same qualitative agreement with the NG predictions as observed for previous measurements in the three-dimensional case, e.g. [29, 30, 35, 36].

Nevertheless, with enhanced accuracy and improved control over systematic effects we see a significant deviation from the NG curves and compare it with the predictions from [18, 19]. Our data is in good agreement with the predicted  $1/R^4$  boundary correction to the effective string theory, even though we cannot exclude the possibility that boundary corrections do not appear until  $\mathcal{O}(R^{-6})$ . If we assume that  $b_2$  does not vanish identically we find evidence that  $b_2$  is small and negative,  $b_2 = -0.5(2)(2)$ , where the first error is

statistical and the second systematic. The resulting curves are in good agreement with the data and it is remarkable that we can describe the data accurately with the predicted splitting. The negative sign of the result is consistent with the sign of the result for confining gauge theories with a weakly curved holographic dual, applied to the case of a string ending on two d-branes [18]. This is the first time that significant deviations from NG energy levels could be observed for open strings in three dimensions. In the case of closed strings and in the finite temperature behavior of the string tension analogous deviations were observed in [26] and [41].

To confirm the findings of this paper it is desirable to check the consistency with earlier results, as e.g. the results for the ground state from [33, 34], and to perform simulations at additional lattice spacings. One would also like to have a precise prediction for the coefficient  $b_2$  to compare with, which is hard to get if  $b_2$  is not constrained by any symmetry. In addition it would be interesting to see whether  $b_2$  is universal or whether it varies between different theories. To clarify the picture one also has to push the simulations to bigger values of  $R$ , in order to reach the region of a convergent expansion for the higher energy levels, and to further increase the precision for the excited states.

## Acknowledgments

The simulations were mainly done on the Linux cluster LC2 at the ZDV of the Johannes Gutenberg-Universität Mainz. A smaller part was done on "Lilly" at the Institut für Kernphysik. I am thankful to the institutes for offering these facilities. The computation of the eigenvalues and the fitting was done using routines from the GNU scientific library [42]. I like to thank P. Majumdar for collaboration on earlier work and discussing and reading early versions of this paper. I also like to thank H. Wittig, H.B. Meyer and G. von Hippel for fruitful discussions and reading the paper. I receive support by the DFG via SFB 443.

## References

- [1] G. S. Bali, *QCD forces and heavy quark bound states*, Phys. Rept. **343**, 1 (2001) [hep-ph/0001312].
- [2] P. Goddard *et. al.*, *Quantum dynamics of a massless relativistic string*, Nucl. Phys. **B 56**, 109 (1973).
- [3] J. Polchinski and A. Strominger, *Effective string theory*, Phys. Rev. Lett. **67**, 1681 (1991).
- [4] J.M. Drummond, *Universal Subleading Spectrum of Effective String Theory*, hep-th/0411017.
- [5] J.M. Drummond, *Reply to hep-th/0606265*, hep-th/0608109.
- [6] N.D. Hari Dass and P. Matlock, *Universality of correction to Luescher term in Polchinski-Strominger effective string theories*, hep-th/0606265.
- [7] N.D. Hari Dass and P. Matlock, *Our response to the response hep-th/0608109 by Drummond*, hep-th/0611215.
- [8] N.D. Hari Dass and P. Matlock, *Field Definitions, Spectrum and Universality in Effective String Theories*, hep-th/0612291.

- [9] F. Maresca, *Comparing the excitations of the periodic flux tube with effective string models*, Ph.D. Thesis, Trinity College, Dublin Ireland (2004).
- [10] N.D. Hari Dass, P. Matlock, Y. Baradwaj, *Spectrum to all orders of Polchinski-Strominger effective String Theory of Polyakov-Liouville Type*, arXiv:0910.5615 [hep-th].
- [11] N.D. Hari Dass, Y. Bharadwaj, *Spectrum to all orders of Polchinski-Strominger effective String Theories of the Drummond Type*, arXiv:0910.5620 [hep-th].
- [12] N.D. Hari Dass, *All Conformal Effective String Theories are Isospectral to Nambu-Goto Theory*, arXiv:0911.3236 [hep-th].
- [13] O. Alvarez, *The Static Potential in String Models*, Phys. Rev. **D24**, 440 (1981).
- [14] J.F. Arvis, *The exact  $q$  anti- $q$  potential in Nambu string theory*, Phys. Lett. **127B**, 106 (1983).
- [15] M. Lüscher, P. Weisz, *Quark confinement and the bosonic string*, JHEP **0207**, 049 (2002) [hep-lat/0207003].
- [16] M. Lüscher and P. Weisz, *String excitation energies in  $SU(N)$  gauge theories beyond the free-string approximation*, JHEP **0407**, 014 (2004) [hep-th/0406205].
- [17] O. Aharony, E. Karzbrun, *On the effective action of confining strings*, JHEP **0906**, 012 (2009) [arXiv:0903.1927 [hep-th]].
- [18] O. Aharony, M. Field, *On the effective theory of long open strings*, arXiv:1008.2636 [hep-th].
- [19] O. Aharony, N. Klinghoffer, *Corrections to Nambu-Goto energy levels from the effective string action*, arXiv:1008.2648 [hep-th].
- [20] H.B. Meyer, *Poincare invariance in effective string theories*, JHEP **0605**, 066 (2006) [arXiv:hep-th/0602281].
- [21] J. Kuti, *Lattice QCD and string theory*, in *Proceedings of the XXIIIrd International Symposium on Lattice field theory*, PoS(Lattice2005), 001 (2005) [hep-lat/0511023].
- [22] J. Juge, J. Kuti and C. Morningstar, *Fine structure of the QCD string spectrum*, Phys. Rev. Lett. **90**, 161601 (2003) [hep-lat/0207004].
- [23] J. Juge, J. Kuti and C. Morningstar, *Excitations of the static quark anti-quark system in several gauge theories*, in *Proceedings of Wako 2003, Color confinement and hadrons in quantum chromodynamics*, 221 (2003) [hep-lat/0312019].
- [24] J. Juge, J. Kuti and C. Morningstar, *QCD string formation and the Casimir energy*, in *Proceedings of Wako 2003, Color confinement and hadrons in quantum chromodynamics*, 233 (2003) [hep-lat/0401032].
- [25] A. Athenodorou, B. Bringoltz and M. Teper, *The Closed string spectrum of  $SU(N)$  gauge theories in 2+1 dimensions*, Phys. Lett. **B656**, 132 (2007) [arXiv:0709.0693 [hep-lat]].
- [26] A. Athenodorou, B. Bringoltz and M. Teper, *Closed flux tubes and their string description in  $D=3+1$   $SU(N)$  gauge theories*, arXiv:1007.4720 [hep-lat] (2010).
- [27] F. Gliozzi, M. Pepe and U. J. Wiese, *The Width of the Confining String in Yang-Mills Theory*, Phys. Rev. Lett. **104**, 232001 (2010) [arXiv:1002.4888 [hep-lat]].
- [28] F. Gliozzi, M. Pepe and U. J. Wiese, *Linear Broadening of the Confining String in Yang-Mills Theory at Low Temperature*, arXiv:1010.1373 [hep-lat] (2010).
- [29] B.B. Brandt and P. Majumdar, *Luscher-Weisz algorithm for excited states of the QCD*

- flux-tube*, in *Proceedings of the XXVth International Symposium on Lattice field theory*, PoS(LAT2007), 027 (2007) [arXiv:0709.3379 [hep-lat]].
- [30] B.B. Brandt, P. Majumdar, *Spectrum of the QCD flux tube in 3d SU(2) lattice gauge theory*, Phys. Lett. **B682**, 253 (2009) [arXiv:0905.4195 [hep-lat]].
  - [31] M. Lüscher and P. Weisz, *Locality and exponential error reduction in numerical lattice gauge theory*, JHEP **0109**, 010 (2001) [hep-lat/0108014].
  - [32] R. Sommer, *A New way to set the energy scale in lattice gauge theories and its applications to the static force and alpha-s in SU(2) Yang-Mills theory*, Nucl. Phys. **B411**, 839 (1994) [hep-lat/9310022].
  - [33] N.D. Hari Dass and P. Majumdar, *Continuum limit of string formation in 3-d SU(2) LGT*, Phys. Lett. **B658**, 273 (2007) [hep-lat/0702019].
  - [34] N.D. Hari Dass and P. Majumdar, *String-like behaviour of 4-D SU(3) Yang-Mills flux tubes*, JHEP **0610**, 020 (2006) [hep-lat/0608024].
  - [35] P. Majumdar, *The String spectrum from large Wilson loops*, Nucl. Phys. **B664**, 213 (2003) [hep-lat/0211038].
  - [36] P. Majumdar, *Continuum limit of the spectrum of the hadronic string*, hep-lat/0406037 (2004).
  - [37] S. Kratochvila, Ph. de Forcrand, *Observing string breaking with Wilson loops*, Nucl. Phys. **B671**, 103 (2003) [hep-lat/0306011].
  - [38] B. Blossier, M. Della Morte, G. von Hippel, T. Mendes and R. Sommer, *On the generalized eigenvalue method for energies and matrix elements in lattice field theory*, JHEP **0904**, 094 (2009) [arXiv:0902.1265 [hep-lat]].
  - [39] G.H. Golub, C.F. Van Loan, *Matrix Computations*, third edition, The Johns Hopkins University Press, Baltimore U.S.A. (1996).
  - [40] M. J. Teper, *SU(N) gauge theories in (2+1)-dimensions*, Phys. Rev. **D59**, 014512 (1999) [hep-lat/9804008].
  - [41] P. Giudice, F. Gliozzi and S. Lottini, *The Confining string beyond the free-string approximation in the gauge dual of percolation*, JHEP **0903**, 104 (2009) [arXiv:0901.0748 [hep-lat]].
  - [42] M. Galassi et al, *GNU Scientific Library Reference Manual*, third edition, ISBN. 0954612078 <http://www.gnu.org/software/gsl/>.